J. Fluid Mech. (2006), *vol.* 568, *pp.* 161–172.
doi:10.1017/S002211200600156X Printed in the United Kingdom

Flipping of an adherent blood platelet over a substrate

By C. POZRIKIDIS

Department of Mechanical and Aerospace Engineering, University of California, San Diego, La Jolla, CA 92093-0411, USA
cpozrikidis@ucsd.edu

(Received 23 September 2005 and in revised form 15 April 2006)

The flipping motion of a blood platelet convected under the action of a simple shear flow over a substrate is discussed. The platelet is modelled as a rigid oblate spheroid with aspect ratio equal to 0.25 whose axis of revolution is perpendicular to the vorticity of the simple shear flow. The particle motion from a given initial position is computed using a boundary element method for Stokes flow based on the double-layer representation. When the platelet is far from the wall, the motion is described by Jeffery's exact solution. As the platelet approaches the wall, the rate of rotation is reduced significantly when the platelet mid-plane is parallel to wall, and mildly when the mid-plane is perpendicular to the wall. Comparison with laboratory data indicates that wall effects alone do not explain the observed slow rate of rotation. It is proposed that a distributed adhesion force imparts to the particle an effective external force and torque at the nominal point of contact, and these slow down the rate of rotation. The process is demonstrated by computing the motion of an adhering platelet whose lowest point is immobilized under the action of a suitable force and torque.

1. Introduction

Blood is a concentrated suspension of red cells, white cells, and platelets, each having a unique constitution and serving a different function. Red cells are highly deformable liquid capsules enclosed by a thin membrane whose resting shape is a biconcave disk, and white cells are viscoelastic spherical particles enclosed by a cortical spherical shell. In the unactivated state, platelets are oblate spheroids with an average aspect ratio approximately equal to 0.25 and diameter approximately equal to 3 μm (Frojmovic & Milton 1982; Frojmovic, Longmire & van de Ven 1990). Like red cells, platelets lack a nucleus; like white cells, platelets exhibits a low degree of flow-induced deformation.

Platelets adhere to injured tissue to initiate the healing process in primary haemostasis. For a platelet to attach to the exposed subendothelium of a blood vessel, the adhesion force must overcome the drag force due to blood flow adjacent to the vessel wall. While the biochemical origin of the adhesion kinetics has been well characterized (e.g. Moroi & Jung 1998; Doggett *et al.* 2002), the non-spherical platelet shape has discouraged the mathematical modelling of the adhesion process by elementary methods of particulate hydrodynamics. Following adhesion, platelets become activated, as evidenced by a drastic change in shape, and coagulate within a growing haemostatic plug. A network of fibrin then develops to stabilize the plug, like

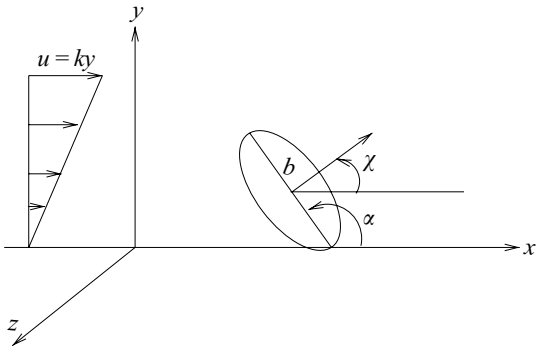

FIGURE 1. Schematic illustration of a platelet flipping over a surface under the action of a simple shear flow.

steel reinforcement, leading to thrombus formation in secondary haemostasis. Under pathological conditions, a large white thrombus consisting of platelets or red thrombus also containing red blood cells develops and separates, possibly causing myocardial infarction and strokes.

Platelets exhibit various degrees of adhesion to activated substrates ranging from weak adherence that allows a continuous particle motion, including rotation and translation, to firm adherence and permanent capture (Frenette *et al.* 1995; Savage, Saldivar & Ruggeri 1996). In the laboratory, spontaneously tethered platelets moving under the influence of a shear flow have been recently observed to exhibit a flipping motion pivoted at a temporary adhesion point around the particle rim (Mody *et al.* 2005). Though arbitrary orientations during the flipping motion are possible, in most cases the platelet axis of revolution remains perpendicular to the vorticity of the shear flow in a left-to-right symmetric configuration. Adhesion is typically initiated when the particle mid-plane is inclined diagonally at the angle $\alpha \simeq 3\pi/4$ with respect to the wall, as illustrated in figure 1. Following one flipping motion, a repetition may occur or else the platelet may dislodge when the particle axis has rotated to an angle of approximately $\alpha \simeq \pi/4$. Adhesion and dislodgement angles depend weakly on the shear rate of the simple shear flow.

A natural point of departure for describing the flipping motion of a platelet over a substrate is Jeffery's (1922) analysis of the motion of an ellipsoid in a general linear flow. When applied to an oblate spheroid in simple shear flow, Jeffery's solution predicts that the particle executes a family of periodic trajectories parametrized by the initial inclination of the unit vector pointing along the particle axis of revolution, called the particle director. When the axis of revolution is perpendicular to the vorticity of the shear flow, the director rotates around the particle centroid with a time-dependent angular velocity describing a full circle. Computations of the motion of a spheroid near a plane wall in this configuration were conducted by Hsu & Ganatos (1994) based on a direct boundary-integral method for large and moderate particle-to-wall separations. In the numerical studies, freely suspended spheroidal particles convected in simple shear flow and heavy or light spheroidal particles settling or rising in an otherwise quiescent fluid were considered. Similar calculations were presented by Gavze & Shapiro (1997, 1998). Pozrikidis (2005) and Mody & King (2005) recently found that a wall in close proximity may prevent the full orbital motion and cause the particle axis to move parallel to the wall or precess around an inclined orientation.

Mody *et al.* (2005) presented a detailed laboratory study of the flipping motion of tethered and free platelets near a plane wall, and developed a pertinent two-dimensional hydrodynamic model. In the theory, the platelet is modelled as a two-dimensional plate that is hinged on the wall at an adhesion point on one end, and is free to rotate under the action of the shear flow at the other end. By superposing the solution of Jeong & Kim (1983) for shear flow past a stationary plate mounted at an arbitrary angle on a infinite plane wall, and the Moffatt (1964) solution for flow in a wedge due to the rotation of one wall, and fixing the value of an adjustable constant, Mody *et al.* derived an evolution equation for the plate inclination angle for vanishing torque, and provided an estimate for the adhesion force.

The objective of this paper is to present a more accurate model of the platelet flipping motion, wherein the equations governing the motion of an oblate spheroid near a wall are solved using a spectral-element method for Stokes flow based on the double-layer representation. The results will show that wall effects alone are not sufficient to describe the slow rotation of the platelet observed in the laboratory. However, accounting for the effect of an adhesion torque imparted to an immobilized particle by a distributed adhesion force reconciles theory and observation.

2. Mathematical formulation and numerical method

We consider the motion of an oblate spheroid with one axis equal to a and two axes equal to b, where $e = a/b < 1$ is the particle aspect ratio. The particle may be freely suspended or subject to a specified force and torque in a semi-infinite simple shear flow along the x-axis above a plane wall located at $y = 0$. The undisturbed velocity field prevailing in the absence of the particle is described by $u_x^\infty = k\,y$, $u_y^\infty = 0$, $u_z^\infty = 0$, where k is the shear rate. The Reynolds number of the flow based on the particle size is assumed to be so small that the motion of the fluid is governed by the linear equations of Stokes flow. In correspondence with laboratory observations of platelet motion by Mody *et al.* (2005), we only consider left-to-right symmetric orientations wherein the particle axis of revolution lies in the (x, y)-plane, as shown in figure 1.

Using the theory of hydrodynamic potentials, we express the velocity field past the particle as a superposition of (*a*) the velocity corresponding to the unperturbed shear flow, $\boldsymbol{u}^\infty$, (*b*) a double-layer potential of Stokes flow defined over the particle surface, and (*c*) the velocity due to a point force and a point torque applied at arbitrary positions inside the particle, as

$$u_j(\boldsymbol{x}_0) = u_j^\infty(\boldsymbol{x}_0) + \iint_{S_p} q_i(\boldsymbol{x})\, T_{ijk}(\boldsymbol{x}, \boldsymbol{x}_0)\, n_k(\boldsymbol{x})\, \mathrm{d}S(\boldsymbol{x}) + v_j(\boldsymbol{x}_0), \tag{2.1}$$

where S_p is the particle surface, $\boldsymbol{q}$ is the vectorial strength density of the Stokes double-layer potential represented by the integral on the right-hand side of (2.1), and $T_{ijk}(\boldsymbol{x}, \boldsymbol{x}_0)$ is the Lorentz Green's function for the stress in a semi-infinite domain of flow bounded by a plane wall where the velocity is required to be zero (Blake 1971; Pozrikidis 1992). The velocity due to the point force, $\boldsymbol{F}$, and point torque, $\boldsymbol{T}$, is given by

$$v_j(\boldsymbol{x}_0) = -\frac{1}{8\pi\mu}\, G_{ji}(\boldsymbol{x}_0, \boldsymbol{X})\, F_i - \frac{1}{8\pi\mu}\, R_{ji}(\boldsymbol{x}_0, \boldsymbol{Y})\, T_i, \tag{2.2}$$

where $G_{ji}(\boldsymbol{x}_0, \boldsymbol{X})$ is the Lorentz Stokes-flow Green's function for the velocity, $R_{ji}(\boldsymbol{x}_0, \boldsymbol{Y})$ is the rotlet representing the velocity field induced by a couplet above

an infinite plane wall, and $\boldsymbol{X}$, $\boldsymbol{Y}$, are arbitrary positions inside the particle. Since $G_{ji}(\boldsymbol{x}_0, \boldsymbol{x}) = 0$, $T_{ijk}(\boldsymbol{x}, \boldsymbol{x}_0) = 0$, and $R_{ji}(\boldsymbol{x}_0, \boldsymbol{x}) = 0$, when $\boldsymbol{x}_0$ lies on the wall, the integral representation (2.1) satisfies the required boundary condition, $\boldsymbol{u}(\boldsymbol{x}_0) = \boldsymbol{0}$, when the field point $\boldsymbol{x}_0$ lies on the wall.

To compute the strength density of the double-layer potential, we let the field point $\boldsymbol{x}_0$ approach the particle surface, and express the limit of the double-layer potential in terms of the principal value, denoted by PV, finding

$$u_j(\boldsymbol{x}_0) = u_j^{\infty}(\boldsymbol{x}_0) + 4\pi\, q_j(\boldsymbol{x}_0) + \iint_{S_p}^{PV} q_i(\boldsymbol{x})\, T_{ijk}(\boldsymbol{x}, \boldsymbol{x}_0)\, n_k(\boldsymbol{x})\, \mathrm{d}S(\boldsymbol{x}) + v_j(\boldsymbol{x}_0). \quad (2.3)$$

Next, we implement the rigid-body-motion boundary condition, $\boldsymbol{u} = \boldsymbol{V} + \boldsymbol{\Omega} \times \hat{\boldsymbol{x}}$, where $\boldsymbol{V}$ is the velocity of translation of the particle surface centroid, $\boldsymbol{x}_c$, $\boldsymbol{\Omega}$ is the angular velocity of rotation about the particle centroid, and $\hat{\boldsymbol{x}} = \boldsymbol{x} - \boldsymbol{x}_c$. Rearranging (2.3), we derive an integral equation of the second kind for $\boldsymbol{q}$,

$$q_j(\boldsymbol{x}_0) = -\frac{1}{4\pi} \iint_{S_p}^{PV} q_i(\boldsymbol{x})\, T_{ijk}(\boldsymbol{x}, \boldsymbol{x}_0)\, n_k(\boldsymbol{x})\, \mathrm{d}S(\boldsymbol{x}) + \frac{1}{4\pi}\big[V_j + \epsilon_{jik}\, \Omega_i\, \hat{x}_{0_k} - u_j^{\infty}(\boldsymbol{x}_0) - v_j(\boldsymbol{x}_0)\big], \quad (2.4)$$

where $\hat{\boldsymbol{x}}_0 = \boldsymbol{x}_0 - \boldsymbol{x}_c$. To complete the boundary integral formulation, we stipulate that the translational and angular velocities of the particle can be derived from the strength density of the double-layer potential as

$$\boldsymbol{V} = -\frac{4\pi}{\mathscr{S}} \iint_{S_p} \boldsymbol{q}\, \mathrm{d}S, \qquad \boldsymbol{\Omega} = \sum_{m=1}^{3} d_m\, \boldsymbol{\omega}^{(m)}, \quad (2.5)$$

where $\mathscr{S}$ is the particle surface area, and

$$d_m = -\frac{4\pi}{A_m}\, \boldsymbol{\omega}^{(m)} \cdot \iint_{S_p} \hat{\boldsymbol{x}} \times \boldsymbol{q}\, \mathrm{d}S \quad (2.6)$$

(Pozrikidis 1992, pp. 133–138). The three vectors, $\boldsymbol{\omega}^{(m)}$, are such that

$$\boldsymbol{v}^{(m)} = \frac{1}{\sqrt{A_m}}\, \boldsymbol{\omega}^{(m)} \times \hat{\boldsymbol{x}}, \quad (2.7)$$

for $m = 1, 2, 3$, represent three orthonormal modes of rigid-body rotation, that is,

$$\big(\boldsymbol{v}^{(q)}, \boldsymbol{v}^{(s)}\big) \equiv \iint_{S_p} \boldsymbol{v}^{(q)} \cdot \boldsymbol{v}^{(s)}\, \mathrm{d}S = \delta_{qs}, \quad (2.8)$$

where δ_{qs} is Kronecker's delta, and

$$A_m = \iint_{S_p} \big(\boldsymbol{\omega}^{(m)} \times \hat{\boldsymbol{x}}\big) \cdot \big(\boldsymbol{\omega}^{(m)} \times \hat{\boldsymbol{x}}\big)\, \mathrm{d}S. \quad (2.9)$$

In practice, the vectors $\boldsymbol{\omega}^{(m)}$ can be found using the Gram–Schmidt orthonormalization process. Zinchenko, Rother & Davis (1997) showed that the angular velocity can be computed directly by substituting (2.7) in (2.8), finding

$$\omega_p^{(q)}\, \mathscr{I}_{pr}\, \omega_r^{(s)} = \delta_{qs}\, A_q, \quad (2.10)$$

where

$$\mathscr{I}_{pr} \equiv \iint_{S_p} (\delta_{pr}|\hat{\boldsymbol{x}}|^2 - \hat{x}_p \hat{x}_r)\, \mathrm{d}S \tag{2.11}$$

is the symmetric surface moment of the inertia tensor. Operating on the second equation of (2.5) and using (2.10), we find

$$\boldsymbol{\Omega} \cdot \mathscr{I} \cdot \boldsymbol{\omega}^{(m)} = d_m A_m = -4\pi\, \boldsymbol{\omega}^{(m)} \cdot \iint_{S_p} \hat{\boldsymbol{x}} \times \boldsymbol{q}\, \mathrm{d}S, \tag{2.12}$$

which shows that the angular velocity can be computed by solving the linear system

$$\mathscr{I} \cdot \boldsymbol{\Omega} = -4\pi \iint_{S_p} \hat{\boldsymbol{x}} \times \boldsymbol{q}\, \mathrm{d}S. \tag{2.13}$$

For a spherical particle of radius a, the vectors $\boldsymbol{\omega}^{(m)}$ can be identified with the unit vectors along three Cartesian axes, yielding $A_m = \frac{8}{3}\pi a^4$ and

$$\boldsymbol{\Omega} = -\frac{3}{2}\left(\frac{4\pi}{\mathscr{S}}\right)^2 \iint_{S_p} \hat{\boldsymbol{x}} \times \boldsymbol{q}\, \mathrm{d}S. \tag{2.14}$$

This simplified expression can also be used for a non-spherical particle with small or moderate aspect ratio, with little effect on the performance of the numerical method.

Subject to the preceding definitions, the adjoint of the integral equation (2.4) admits an eigensolution that is proportional to the normal vector, $\boldsymbol{n}$. To remove this eigenfunction and thus allow a solution by the method of successive substitutions, we add a deflating term to the right-hand side of (2.4) and derive the modified integral equation

$$q_j(\boldsymbol{x}_0) = -\frac{1}{4\pi} \iint_{S_p}^{PV} q_i(\boldsymbol{x})\, T_{ijk}(\boldsymbol{x}, \boldsymbol{x}_0)\, n_k(\boldsymbol{x})\, \mathrm{d}S(\boldsymbol{x}) + \frac{1}{\mathscr{S}}\, n_j(\boldsymbol{x}_0) \iint_{S_p} \boldsymbol{q} \cdot \boldsymbol{n}\, \mathrm{d}S$$
$$+ \frac{1}{4\pi}\big[V_j + \epsilon_{jik}\, \Omega_i\, \hat{x}_{0_k} - u_j^{\infty}(\boldsymbol{x}_0) - v_j(\boldsymbol{x}_0)\big], \tag{2.15}$$

where the point $\boldsymbol{x}_0$ lies on the particle surface (Pozrikidis 1992, pp. 133–138). Projecting (2.15) onto the normal vector, $\boldsymbol{n}(\boldsymbol{x}_0)$, integrating over the particle surface, and using an integral identity, we find $\int\int_{S_p} \boldsymbol{q} \cdot \boldsymbol{n}\, \mathrm{d}S = 0$, which shows that the solution of (2.15) also satisfies (2.3).

In the present implementation, the integral equation was solved using the spectral boundary-element method discussed by Pozrikidis (2005) to yield the particle translational and angular velocities. Once these are available, the equations governing the particle centroid motion and director orientation angle are integrated in time using the Runge–Kutta method with a constant time step, $k\Delta t = 0.02$. In the majority of the computations, the isoparametric quadratic expansion was used, and the particle surface was discretized into 128 elements, as shown in figure 2(*a*). Each simulation consumes approximately 4 h of CPU time on an Intel 2.0 GHz processor. To confirm the accuracy of the results, a limited number of computations were performed with 512 elements, as shown in figure 2(*b*), at a computational cost of 48 h.

3. Results and discussion

A set of simulations was conducted for freely suspended oblate spheroids with aspect ratio $e = 0.25$, in the absence of an adhesion force or torque. At the initial

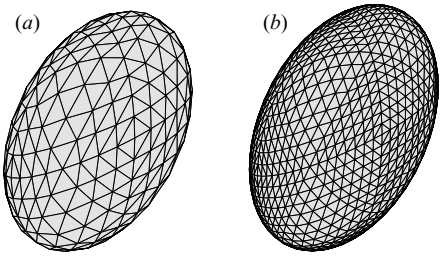

FIGURE 2. Discretization of the surface of a platelet with aspect ratio 0.25 into (*a*) 128 or (*b*) 512 quadratic elements, each defined by six nodes.

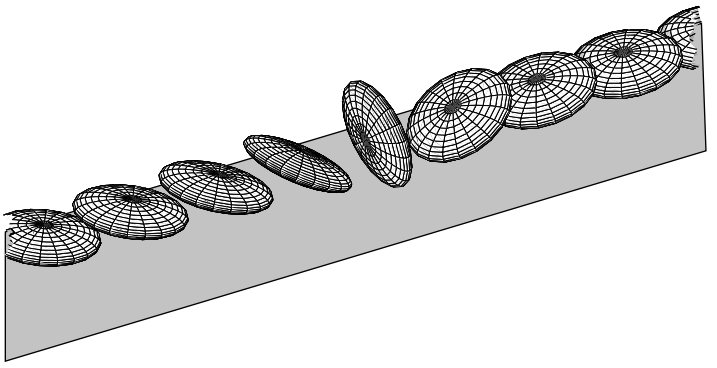

FIGURE 3. Flipping motion of a platelet over a plane wall under the influence of a simple shear flow. In the vertical orientation, the platelet is nearly in contact with the wall.

instant, the particle centre is placed at a distance d above the wall, with the particle director lying in the (x, y)-plane perpendicular to the wall; with reference to figure 1, $\chi = \pi/2$ and $\alpha = \pi$. When the distance, d, is much larger than the particle size, the particle centroid is advected with the local velocity of the simple shear flow, while the angle χ evolves according to Jeffery's differential equation

$$\Omega_z = \frac{\mathrm{d}\chi}{\mathrm{d}t} = -\frac{k}{2}\left(1 - \frac{e^2-1}{e^2+1}\cos(2\chi)\right), \tag{3.1}$$

where Ω_z is the particle angular velocity around the z-axis about the particle centre. Integrating this equation by analytical methods, we find that the particle exhibits periodic rotation with period $T_\infty = (2\pi/k)\,(e + 1/e)$. Figure 3 illustrates the particle motion for $d/b = 0.94$. For this initial position, when the particle rotates and reaches the vertical orientation, the particle rim nearly touches the wall.

Figure 4(*a*) shows the trajectory of the particle centre for $d/b = 0.94$ (solid line), 1.0, 1.1, 1.25, and 1.50 (broken lines), computed with 128 boundary elements, and figure 4(*b*) shows the evolution of the minimum distance of the particle rim from the wall. The hardly visible dotted line tracing the solid line duplicates the calculation for $d/b = 0.94$ with 512 boundary elements, included to demonstrate that the numerical error is small. In all graphs shown in figure 4, time has been shifted so that, at $t = 0$, the particle director is parallel to the wall and the platelet mid-plane is perpendicular to the wall, $\chi = 0$ and $\alpha = \pi/2$. Figure 4(*b*) shows that, when $d/b = 0.94$, the minimum distance is approximately 1% of the particle diameter. Because of the high curvature of the graphs at the origin, the rim is close to the wall only for a limited period of time that lasts a fraction of the inverse shear rate. Thus, unlike a spherical particle

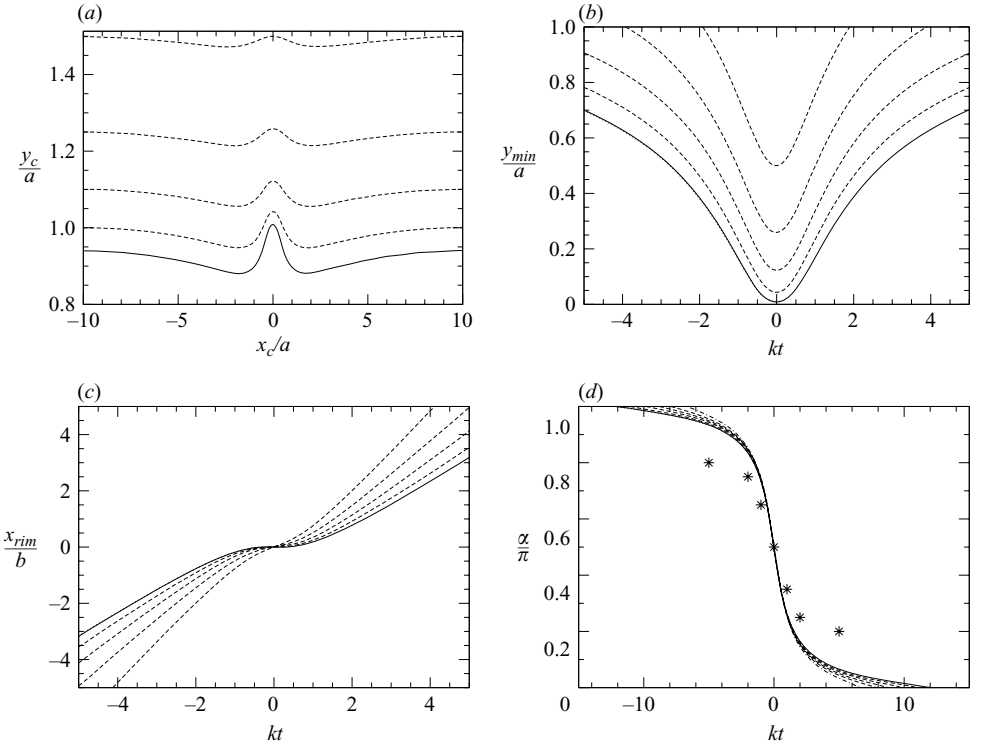

FIGURE 4. (*a*) Trajectory of the particle centre in the (x, y)-plane for $d/b = 0.94$ (solid line), 1.0, 1.1, 1.25, and 1.50 (dashed lines). (*b, c*) Evolution of the minimum distance and corresponding streamwise position of the particle rim from the wall. (*d*) Evolution of the platelet inclination angle, α, over one period, for $d/b = 0.94$ (solid line), 1.0, 1.1, 1.25, 1.50 (dashed lines), and ∞ (dot-dashed outermost line). The asterisks correspond to the laboratory data of Mody *et al.* (2005) for freely suspended platelets near rotating near a substrate. The hardly visible dotted lines tracing the solid lines duplicate the calculation for $d/b = 0.94$ with a high number of surface elements.

modelling a leukocyte, a freely suspended platelet strongly interacts with the wall only when it is sufficiently close to the vertical configuration. Figure 4(*c*) illustrates the evolution of the streamwise position of the lowest point of the particle rim, showing that the nominal point of contact with the wall is nearly stationary over a limited period of time. Accordingly, the slip velocity is small when the particle is nearly perpendicular to the wall.

Figure 4(*d*) shows the evolution of the platelet inclination angle, α, defined in figure 1, for $d/b = 0.94$ (solid line), 1.0, 1.1, 1.25, and 1.50 (dashed lines). The Jeffery solution corresponding to $d/b = \infty$ and described by (3.1) is represented by the outermost dot-dashed line. The results confirm that the particle motion is periodic, and the wall has a significant influence on the period of the motion, T. For $d/b = 0.94$, 1.0, 1.1, 1.25, 1.50, and ∞, we find $kT = 48.8$, 44.2, 39.3, 35.2, 31.7, and 26.7, respectively. Thus, when the particle is in near contact with the wall in the vertical orientation, the period is nearly twice the Jeffery period for infinite shear flow. Net particle migration away from the wall does not occur, in compliance with reversibility of Stokes flow. The mean velocity of particle translation relative to that in the absence of the wall is defined as $v_x = \Delta x/(kTd)$, where Δx is the distance that the particle centroid has

travelled over one period. We find that, as d/b increases from 0.94 to 1.50, v_x increases from 0.93 to 0.98, and tends to unity as d/b tends to infinity. Thus, the wall has a significant but not profound effect on the rate of particle translation.

Figure 4(d) shows that the wall has only a minor effect on the particle rate of rotation in the vertical orientation, $\alpha \simeq \pi/2$. In fact, the effect of the wall is small for all inclinations of interest to platelet adhesion, $\pi/4 < \alpha < 3\pi/4$. The asterisks in figure 4(d) correspond to the laboratory data of Mody *et al.* (2005) for freely suspended platelets convected near the substrate, extracted from their figure 6. Though the actual data exhibit a significant amount of scattering, the asterisks faithfully reproduce the main trends. To reconcile the noticeable difference between Jeffery's theoretical predictions and the experimental values, Mody *et al.* (2005) implemented an approximate correction to the Jeffery orbit. The correction effectively extrapolates the slow rate of rotation observed when the platelet is parallel to the wall, $\chi = \pi/2$ and $\alpha = \pi$, to intermediate inclinations. The correction factor is based on the resistance coefficient for rotation of a zero-thickness circular disk calculated by Kim *et al.* (2001). The present results suggest that the effect of the wall is not sufficiently strong to justify this substantial correction and reconcile theory and observation. Thus, hydrodynamic wall effects alone are not sufficient to explain the slow rotation of a platelet flipping over a plane wall.

A more realistic model of the flipping motion of an adherent platelet takes into consideration the narrowly distributed adhesion force developing between the lowest part of the platelet and the wall. Mody *et al.* (2005) superposed the solution of Jeong & Kim (1983) for shear flow past a stationary infinite plate mounted at an arbitrary angle on a infinite plane wall, and the Moffatt (1964) solution for flow in a wedge due to the rotation of one wall, to derive an evolution equation for the plate inclination angle for the condition of vanishing torque. This model involves an adjustable constant that was set to achieve the best fit with the laboratory data. The force acting on the rotating plate has a radial component with respect to the point of contact and an azimuthal component normal to the plate in the (x, y)-plane. The authors assumed that receptor-ligand bonds align in the radial direction, and found that the adhesion force is repulsive when $0 < \chi < \pi/2$, promoting bond formation, attractive when $-\pi/2 < \chi < 0$, promoting bond dissociation, and zero when $\chi = 0$ whereupon the platelet is oriented perpendicular to the wall. However, some bonds must be oriented in the azimuthal direction to cancel the azimuthal component of hydrodynamic force and immobilize the lowest point of the particle rim.

An improved model can be built on the realization that a distributed adhesion force developing near the point of contact imparts to the particle a net force of a suitable magnitude and orientation in the (x, y)-plane, and a net torque around the z-axis about the point of contact. The adhesion force is such that the lowest point of the platelet rim is immobilized during the motion, while the adhesion torque opposes the clockwise rotation. Since we have found that the hydrodynamic effect of the wall is weak, an approximate differential equation governing the particle rotation for angles $-\pi/4 < \chi < \pi/4$ is Jeffery's equation (3.1) with the adhesion term, $k\,\mathscr{F}(\chi)$, added to the right-hand side, where $\mathscr{F}(\chi)$ is a dimensionless function expressing the effect of the adhesion torque. Figure 5(a) shows the predictions of this model for an idealized case where the function $\mathscr{F}$ is assumed to be constant. The prediction for $\mathscr{F} \simeq 0.4$ is a good fit to the experimental data of Mody *et al.* (2005) represented by the asterisks. To estimate the magnitude of the adhesion torque, T_z, we relate it to the aforementioned dimensionless torque, $\mathscr{F}(\chi)$, by the equation $\mathscr{F} = T_z(\chi)/(6\pi\mu R_z k b^3)$, where R_z is a dimensionless resistance coefficient for rotation. We performed a

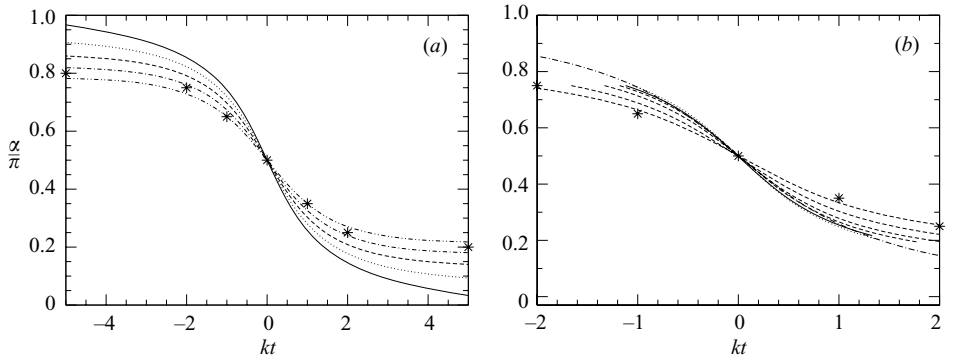

FIGURE 5. Effect of an adhesion torque applied at the point of contact on the rotation of a platelet. (*a*) Modification of the Jeffery trajectory for $\mathscr{F} = 0$ (solid line), 0.1, 0.2, 0.3, and 0.4 (dashed double-dot line). (*b*) Numerical solutions for an adhering platelet subject to adhesion torque $T_z/(\mu k b^3) = 0$ (solid line), and 2, 5, 10, 15 (dashed lines), all for $d/b = 0.80$; the dot-dashed line represents the Jeffery solution in the absence of a wall, and the dotted line is the numerical solution for zero torque and $d/b = 0.85$. The asterisks correspond to the laboratory data of Mody *et al.* (2005).

computation using the standard boundary-integral equation for Stokes flow based on the single-layer representation included in the public library *BEMLIB* (Pozrikidis 2002), and found that, in the vertical orientation, $\chi = 0$ and $\alpha = \pi/2$, the resistance coefficient is $R_z = 2.20$. An estimate for the adhesion torque can be obtained by writing $T_z/(\mu k b^3) = 6\pi R_z \mathscr{F}$ and taking $\mathscr{F} \simeq 0.4$ according to figure 5(*a*), which yields $T_z/(\mu k b^3) \simeq 16.6$. However, the results of this calculation only pertain to the conditions and materials of the experiment corresponding to the data.

To study the motion in more precise terms and also compute the magnitude of the adhesion force developing during the rotation, a set of simulations was carried out where the particle director at the initial instant is inclined diagonally at the angle $\chi = \pi/4$. The x and y components of the adhesion force were computed at every instant for the condition that the x and y velocity components of the lowest point of the particle rim are zero, that is, the nominal contact point is stationary. For lack of a better alternative, the adhesion torque was assumed to be constant during the rotation. In the numerical method, the stationary-rim condition is added as a linear constraint in the boundary integral equation discussed in § 2. The constrained problem requires nearly four times the CPU time as the unconstrained problem in the absence of adhesion. Figure 6 illustrates the particle rotation for initial centre-to-wall separation $d/b = 0.8$, corresponding to initial particle-to-wall gap $y_{min}/b = 0.093$. Comparing this illustration to that shown in figure 3 for a freely convected particle, we clearly see the immobilizing effect of adhesion.

Figure 5(*b*) shows the effect of the adhesion torque on the particle rotation for initial particle centre elevation $d/b = 0.8$. The Jeffery solution for a torque-free particle suspended in infinite shear flow is represented by the dot-dashed line. To assess the effect of the particle-to-wall separation, the solution for $d/b = 0.85$ and vanishing torque is also shown as a dotted line. The solid, dotted, and dot-dashed curves, all for zero torque, nearly coincide due to the demonstrated weak effect of the wall. The prediction for adhesion torque, $T_z/(\mu k b^3) = 15$, fits well the experimental data of Mody *et al.* (2005) represented by the asterisks. This value of the torque is in fair

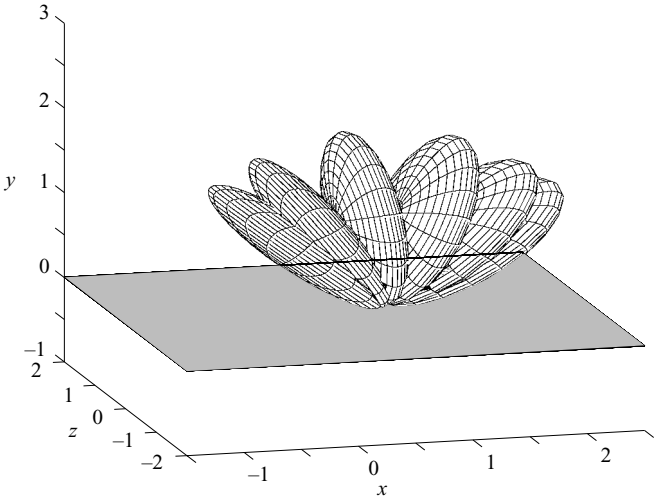

FIGURE 6. Rotation of a torque-free adhering platelet around the lowest point of the rim displayed at equal time intervals.

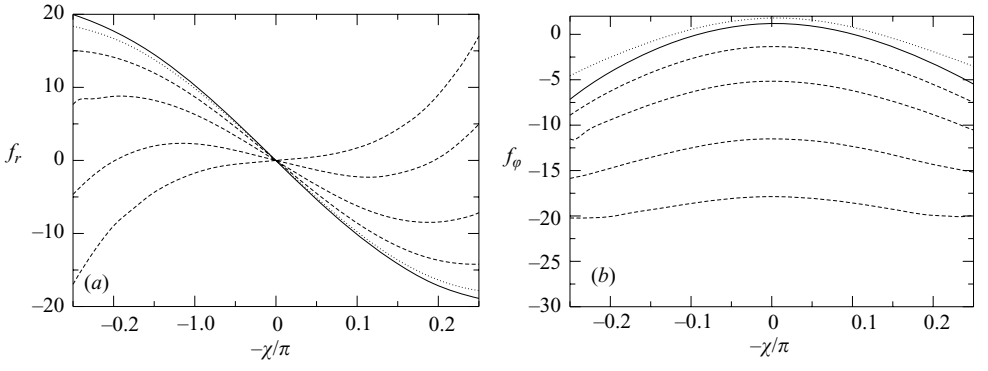

FIGURE 7. (*a*) Radial and (*b*) azimuthal adhesion force coefficients for adhesion torque $T_z/(\mu k b^3) = 0$ (solid line), and 2, 5, 10, 15 (dashed lines), all for $d/b = 0.80$; the dotted line is the numerical solution for zero torque and $d/b = 0.85$.

agreement with the aforementioned theoretical estimate based on the modification of the Jeffery orbit equation with $\mathscr{F} = 0.4$.

Figure 7 illustrates the radial and azimuthal components of the adhesion force exerted on the particle, necessary to immobilize the point of rotation, for several values of the adhesion torque. The force coefficients shown are defined as $f_r = F_r/(\mu k b^2)$ and $f_\varphi = F_\varphi/(\mu k b^2)$. As expected from geometrical symmetry, the radial component of the force is zero in the vertical orientation, $\chi = 0$, whereas the azimuthal component achieves a local maximum. For zero torque, the radial component of the force is positive during the first part of the rotation, $0 < \chi < \pi/4$, and negative during the second part of the rotation, $-\pi/4 < \chi < 0$. Thus, the adhesion force pushes the particle away from the wall when $-\pi/4 < \chi < 0$, and pulls the particle toward the wall when $0 < \chi < \pi/4$. The two-dimensional flap model of Mody *et al.* (2005, figure 4) predicts a similar behaviour, but with a substantially lower maximum radial force $f_r \simeq 0.75 \times 2\pi = 4.712$ occurring when $\chi = -\pi/4$, whereas we find $f_r \simeq 20$. The

four-fold difference can be attributed to an adjustable parameter involved in the two-dimensional model. As the adhesion torque is increased, the magnitude of the radial force decreases, as the induced particle rotation tends to counterbalance the rotation due to the simple shear flow. At high adhesion torques, the radial force becomes negative in the first part of the rotation, $0 < \chi < \pi/4$, and positive in the second part of the rotation, $-\pi/4 < \chi < 0$.

4. Discussion

Frenette *et al.* (1995) observed that platelets roll over the venular endothelium with a wide range of velocities by executing a sequence flipping motions. Savage *et al.* (1996) reported small migration velocities on a different substrate and stated they were unable to discern the detailed nature of the particle motion. These studies suggest that the strength of the adhesion forces and torque, as determined by the biochemistry of the adhesion bonds, is an important aspect of the biophysics of the motion. We have found that, in the absence of adhesion force and torque, the hydrodynamic component of the platelet flipping motion can be accurately described by Jeffery's (1922) exact solution even in close proximity to a substrate, but the predicted rate of rotation substantially differs from that reported by Mody *et al.* (2005). Including an adhesion force and torque, and computing the force for the condition of platelet rim adhesion, considerably improves the agreement. The motion of an adhering platelet is successfully described by a simple modification of the Jeffery equation involving an additional term that slows down the rate of rotation.

A comprehensive description of the individual platelet motion must involve a molecular adhesion component. Fogelson & Guy (2004) developed a continuum (volume averaged) model for platelet aggregation, wherein platelet–wall adhesion forces are computed in terms of the volume concentration of reactive sites on the wall, complemented by transport equations for the concentration of activated and non-activated platelets in the suspension. Agresal *et al.* (1998) developed numerical methods for computing the interaction of adhering suspended cells, and modelled bond formation and breakup in terms of a reversible reaction kinetics at equilibrium. The bonds themselves are regarded as springs with a specified equilibrium length oriented from one adhesion site on one cell to another adhesion site on another cell. Hodges & Jensen (2002) used a similar method to study the spreading and peeling dynamics of a cell on a plane surface, assuming that the bonds are oriented perpendicular to the wall. In the most sophisticated molecular adhesion models, the equations governing the rate of bond association and dissociation involve the wall shear rate and shear stress (e.g. Alon *et al.* 1997). Such molecular models have been combined with hydrodynamics to describe the rolling of solitary white cell or a collection of cells represented as spherical particles (Hammer & Apte 1992; King & Hammer 2001). The implementation of such models to platelet adhesion on a substrate is being considered in current work.

This research was supported by a grant provided by the National Science Foundation.

REFERENCES

Agresar, G., Linderman, J. J., Tryggvason, G. & Powell, K. G. 1998 An adaptive, Cartesian, front-tracking method for the motion, deformation and adhesion of circulating cells. *J. Comput. Phys.* **143**, 346–380.

Alon, R., Chen, S., Puri, K. D., Finger, E. B. & Springer, T. A. 1997 The kinetics of L-selectin tethers and the mechanics of selectin-mediated rolling. *J. Cell Biol.* **138**, 1169–1180.

Blake, J. R. 1971 A note on the image system for a Stokeslet in a no-slip boundary. *Proc. Camb. Phil. Soc.* **70**, 303–310.

Doggett, T. A., Girdhar, G., Lawshé, A., Schmidtke, D. W., Laurenzi, I. J., Diamond, S. L. & Diacovo, T. G. 2002 Selectin-like kinetics and biomechanics promote rapid platelet adhesion in flow: The GPIbα-vWF Tether Bond. *Biophys. J.* **83**, 194–205.

Fogelson, A. & Guy, R. D. 2004 Platelet wall interactions in continuum models of platelet thrombosis: formulation and numerical solution. *Math. Med. Biol.* **21**, 293–334.

Frenette, P., Johnson, R. C., Hynes, R. O. & Wagner, D. D. 1995 Pletelets roll on stimulated endothelium in vivo: An interaction mediated by endothelial P-selectin. *Proc. Natl Acad. Sci. USA* **92**, 7450–7454.

Frojmovic, M. M., Longmire, K. & van de Ven, T. G. M. 1990 Long-range interactions in mammalian platelet aggregation. and disease. *Biophys. J.* **58**, 309–318.

Frojmovic, M. M. & Milton, J. G. 1982 Human platelet size, shape, and related functions in health and disease. *Physiol. Rev.* **62**, 185–261.

Gavze, E. & Shapiro, M. 1997 Particles in shear flow near a solid wall: effect of nonsphericity on forces and velocities. *Intl J. Multiphase Flow* **23**, 155–182.

Gavze, E. & Shapiro, M. 1998 Motion of inertial spheroidal particles in a shear flow near a solid wall with special application to aerosol transport in microgravity. *J. Fluid Mech.* **371**, 59–79.

Hammer, D. A. & Apte, S. M. 1992. Simulation of cell rolling and adhesion on surfaces in shear flow: general results and analysis of selectin-mediated neutrophil adhesion. *Biophys. J.* **62**, 35–57.

Hodges, S. R. & Jensen, O. E. 2002 Spreading and peeling dynamics in a model of cell adhesion. *J. Fluid Mech.* **460**, 381–409.

Hsu, R. & Ganatos, P. 1994 Gravitational and zero-drag motion of a spheroid adjacent to an inclined plane at low Reynolds number. *J. Fluid. Mech.* **268**, 267–292.

Jeffery, G. B. 1922 The motion of ellipsoidal particles immersed in a viscous fluid. *Proc. R. Soc. Lond.* A **102**, 161–179.

Jeong, J. & Kim, M. 1983 Slow viscous flow around an inclined fence on a plane. *J. Phys. Soc. Japan* **52**, 2356–2363.

Kim, M.-U., Kim, K. W., Cho, Y.-H. & Kwak, B. M. 2001 Hydrodynamic force on a plate near the plane wall. Part I: plate in sliding motion. *Fluid Dyn. Res.* **29**, 137–170.

King, M. R. & Hammer, D. A. 2001 Multiparticle adhesive dynamics. Interactions between stably rolling cells. *Biophys. J.* **81**, 799–813.

Mody, N. & King, M. R. 2005 Three-dimensional simulations of a platelet-shaped spheroid near a wall in shear flow. *Phys. Fluids* **17**, 113302.

Mody, N. A., Lomakin, O., Doggett, T. A., Diacovo, T. G. & King, M. R. 2005 Mechanics of transient platelet adhesion to von Willebrand factor under flow. *Biophys. J.* **88**, 1432–1443.

Moffatt, H. K. 1964 Viscous and resistive eddies near a sharp corner. *J. Fluid Mech.* **18**, 1–18.

Moroi, M. & Jung, S. M. 1998 Integrin-mediated plateled adhesion. *Frontiers in Bioscience* **3**, d719–728.

Pozrikidis, C. 1992 *Boundary Integral and Singularity Methods for Linearized Viscous Flow*. Cambridge University Press.

Pozrikidis, C. 2002 *A Practical Guide to Boundary-Element Methods with the Software Library BEMLIB*. Chapman & Hall/CRC.

Pozrikidis, C. 2005 Orbiting motion of a freely-suspended spheroid near a plane wall. *J. Fluid Mech.* **541**, 105–114.

Savage, B., Saldivar, E. & Ruggeri, A. M. 1996 Initiation of platelet adhesion by arrest into fibrogen or translocation on von Willebrand factor. *Cell* **84**, 289–297.

Zinchenko, A. Z., Rother, M. A. & Davis, R. H. 1997 A novel boundary-integral algorithm for viscous interaction of deformable drops. *Phys. Fluids* **9**, 1493–1511.